SAC/EPSA/CVD/SR/2020/02

Absolute radiometric performance of INSAT-3D and INSAT-3DR Visible and SWIR channels over desert site

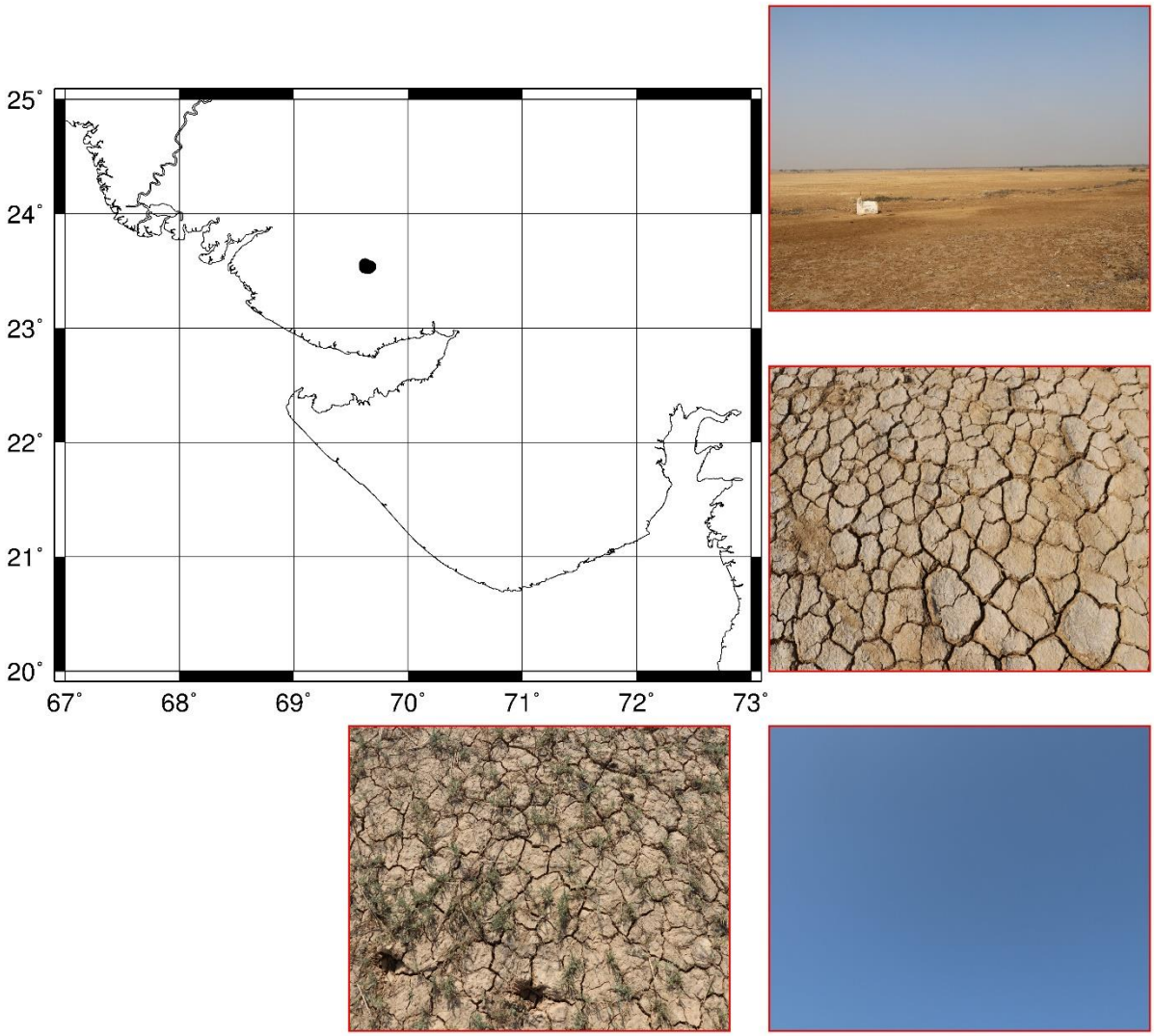

K. N. Babu[1], Mahesh C[1], Nandkishor Kumawat[1], Ashim Kumar Mitra[2], Rakesh Kumar[2]

20/05/2020

[1]Calibration and Validation Division (CVD)
Earth, Ocean, Atmosphere, Planetary Sciences & Applications Area (EPSA)
Space Applications Centre (ISRO)
Ahmedabad – 380 015

[2]India Meteorological Department, New Delhi

Document control sheet

1	Report No.	SAC/EPSA/CVD/SR/2020/02
2	Publication Date	May, 2020
3	Title	Absolute radiometric performance of INSAT-3D and INSAT-3DR Visible and SWIR channels over desert site
4	Type of report	Scientific
5	Number of pages	25
6	Authors	K. N. Babu, Mahesh C, Nandkishor Kumawat, Ashim Kumar Mitra, Rakesh Kumar
7	Originating unit	CVD/EPSA
8	Abstract	This document describes the radiometric performance of the visible (VIS) and shortwave infrared (SWIR) channels of INSAT-3D and INSAT-3DR imager, based on vicarious calibration computation carried out using the ground measured reflectance and atmospheric parameters over the quasi-homogenous desert conditions (Great Rann of Kutchchh) during winter season for four clear-sky days.
9	Key words	Radiance, homogeneous, reflectance, uncertainty, Vicarious Calibration
10	Security classification	Unrestricted
11	Distribution statement	Among all concerned

Contents

Table of Contents

List of Figures

List of Tables

1. Abstract

A calibration campaign conducted over Greater Rann of Kutchchh (GROK) to make synchronous measurements of surface reflectance and other atmospheric variables like, aerosol optical depth, integrated water vapor and columnar ozone to carryout the post launch radiometric performance assessment of INSAT-3D and INSAT-3DR visible and SWIR channels. As the campaign happened in winter season, atmospheric condition favors with less anthropogenic activities and considerable solar illumination. We carried out systematic measurements for the radiance simulation using radiative transfer model along with measured atmospheric variables. The field campaign lasted for five days and only four days of measurements were used for the study, as one-day was disturbed by induced western disturbance which was persisted throughout the day for the campaign site.

In this analysis it is observed the relative errors of the VIS bands of INSAT-3D and INSAT-3DR imager are within 44% and 23% respectively when compared with the RT simulated TOA radiance values. However, the results also show that the relative errors of the SWIR bands of INSAT-3D and INSAT-3DR imager are within 5.6% and 14.3% respectively. Overall, the results of the vicarious radiometric calibration obtained using the ground reflectance-based approach have been demonstrated that the IMAGER onboard the INSAT-3D/3DR satellite displays substantial degradation in radiometric performance, particularly at VIS channel during this study.

The correlation between INSAT-3D derived TOA radiance and 6SV simulated radiance is 0.79 (visible) and 0.76 (SWIR). The estimated RMSE value is found to be high 31.54 $Wm^{-2}sr^{-1}\mu m^{-1}$ for IMG-VIS band and 1.43 $Wm^{-2}sr^{-1}\mu m^{-1}$ IMG-SWIR band. The estimated absolute bias and relative error between the satellite measured radiance and 6SV simulated radiance are 30.96$Wm^{-2}sr^{-1}\mu m^{-1}$ (43.85%) and 1.17$Wm^{-2}sr^{-1}\mu m^{-1}$ (5.61%) for VIS and SWIR bands respectively. The correlation between INSAT-3DR measured radiance and 6SV simulated radiance for IMG-VIS/IMG-SWIR are 0.83/0.87. The absolute bias values are 16.79$Wm^{-2}sr^{-1}\mu m^{-1}$ and 2.97$Wm^{-2}sr^{-1}\mu m^{-1}$ for INSAT-3DR VIS and SWIR with relative percentage errors 17.15% and 3.05% respectively.

2. Introduction

Primary purpose of INSAT-3D/-3DR mission is to meet the nation's need for meteorological and oceanic monitoring applications, and rescue services. INSAT-3D/-3DR is an advanced weather satellite of India configured with improved imaging system and atmospheric sounder as compared to earlier missions (INSAT-3A and KALPANA-1). Monitoring the radiometric calibration of satellite sensors is an essential step in the estimation of reliable geo-physical products and continuous usage for various quantitative applications. This radiometric calibration, which converts the electronic digital number (DN) values to physical units (radiance), has been performed to acquire consistently accurate radiometric information over a specifically designed sensor's lifetime (Belward, 1999; Liang, 2004). To secure radiometric calibration and the continuity of satellite data from multiple sensors, pre- and post-launch calibration have been proposed during the mission phase to determine the characteristics/performance of radiometric calibration (Butler, and Barnes, 1998; Dinguirard, M., and Slater, P. A., 1999). The pre-calibration step, which is conducted in a controlled laboratory setting, uses

a well-characterized radiant source. However, because calibrated sensors undergo degradation by the severe environmental conditions which are encountered after launch (Hagolle, 1999), operational space-borne satellites need to be monitored to obtain their absolute radiometric characteristics when in orbit. For in-flight calibration of satellites, on-board, vicarious, lunar, and cross-calibration techniques have been suggested for radiometric calibration. On-board calibration is performed in orbiting satellites using well-known sources such as artificial lamps or the sun. On-board calibrators have the advantage of allowing frequent response determinations. However, they increase the cost and weight of total satellite instruments. Vicarious and cross-calibration techniques are used for systems which are not having on-board calibrators. The vicarious calibration techniques relying on *in-situ* characterizations of surface targets, eventually, field campaigns are conducted over different desert sites. Other input parameters are also collected for the radiative transfer model simulation (e.g., atmospheric constituents, such as aerosol optical depth, ozone column, and water vapor content) using well calibrated spectroradiometer, sunphotometer, ozonemonitor and etc.

This report summarizes in details the radiometric perform of INSAT-3D and -3DR visible and SWIR channels over the quasi-uniform desert target during Indian winter season.

3. INSAT-3D & -3DR Multi-spectral Imager

INSAT-3D & 3DR carry multi-spectral Imager (optical radiometer) capable of generating the images of the earth in six wavelength bands significant for meteorological observations, namely, visible, shortwave infrared, middle infrared, water vapor and two bands in thermal infrared regions. Imager will generate images of the earth disk from geostationary altitude of 36,000 km every 30 minutes and provide information on various parameters, namely, outgoing long-wave radiation, quantitative precipitation estimation, sea surface temperature, snow cover, cloud motion winds, etc. Imager payload is an improved version of VHRR flown on INSAT-3A and Kalpana-1 satellites with significant improvements in spatial resolution, number of spectral channels and functionality. The INSAT-3DR Imager payload is a replica of INSAT-3D Imager, the sensor specifications (center wavelength, band coverage, and resolution) is given in Table 1.

Table 1. Specifications of INSAT-3D/3DR imager (Bands, center wavelength, band coverage, and associated spatial resolution)

Band No.	Description	Center Wavelength (µm)	Band coverage (µm)	Resolution (km)
1	VIS(Visible)	0.65	0.55 - 0.75	1
2	SWIR(Short Wave Infrared)	1.625	1.55 - 1.70	1
3	MWIR (Mid Wave Infrared)	3.9	3.80 - 4.00	4
4	WV (Water Vapor)	6.75	6.50 - 7.00	8
5	TIR-1 (Thermal Infrared)	10.7	10.2 - 11.2	4
6	TIR-2 (Thermal Infrared)	12	11.5 - 12.5	4

4. Calibration site and Field campaign measurements

The selection of a calibration and validation (Cal-Val) site for vicarious radiometric Calibration/validation has very important role when using reflectance-based, irradiance-based, or

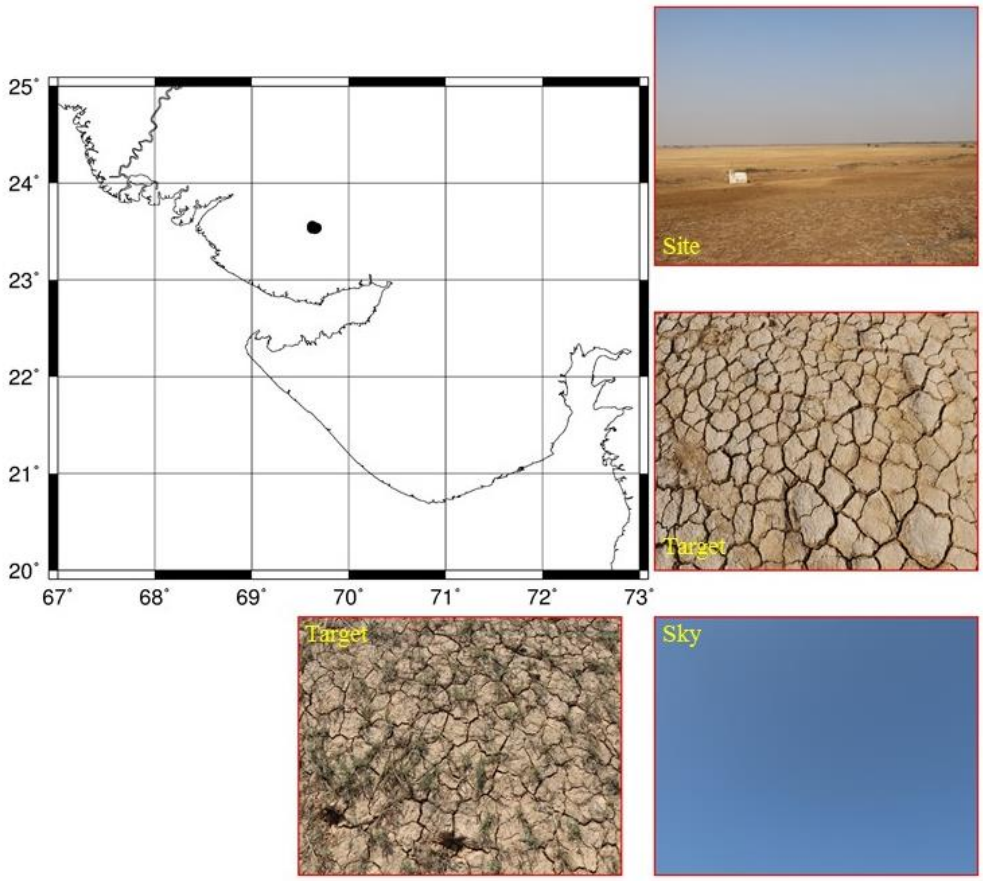

Figure 1. The study region and the sites of calibration campaign.

Table 2. Instruments used during the calibration campaign.

Instrument name	Serial no.	Make
Hyper-spectral radiometer	HR4-18443	Analytical Spectral Device
Sun-photometer	MicroTOPSII-22446	Solar light
Ozonometer	MicroTOPSII-19722	Solar light
Spectralon panel	18443 (Secondary)	Labs Sphere
Spectralon panel	18446 (Master)	Labs Sphere

radiance-based approaches. In this study, the Greater Rann of Kutchchh (GROK) site in Gujarat, is selected as our vicarious radiometric calibration site. The measurement target site is midway to white

desert about 40 km away from Bhuj, Gujarat with an altitude of ~4 meter above the mean sea level (Figure 1). Center of the site was used for calibration campaign, which is located at 23.5218ºN and 69.6511ºE. The site is extended upto ~20km^2 area, presenting a flat, dry and little shrubs characterizing from moderate to high reflectance surface target. The site location, ground and sky condition during the campaign is shown in **Figure 1** and the list of instruments used in **Table 1**.

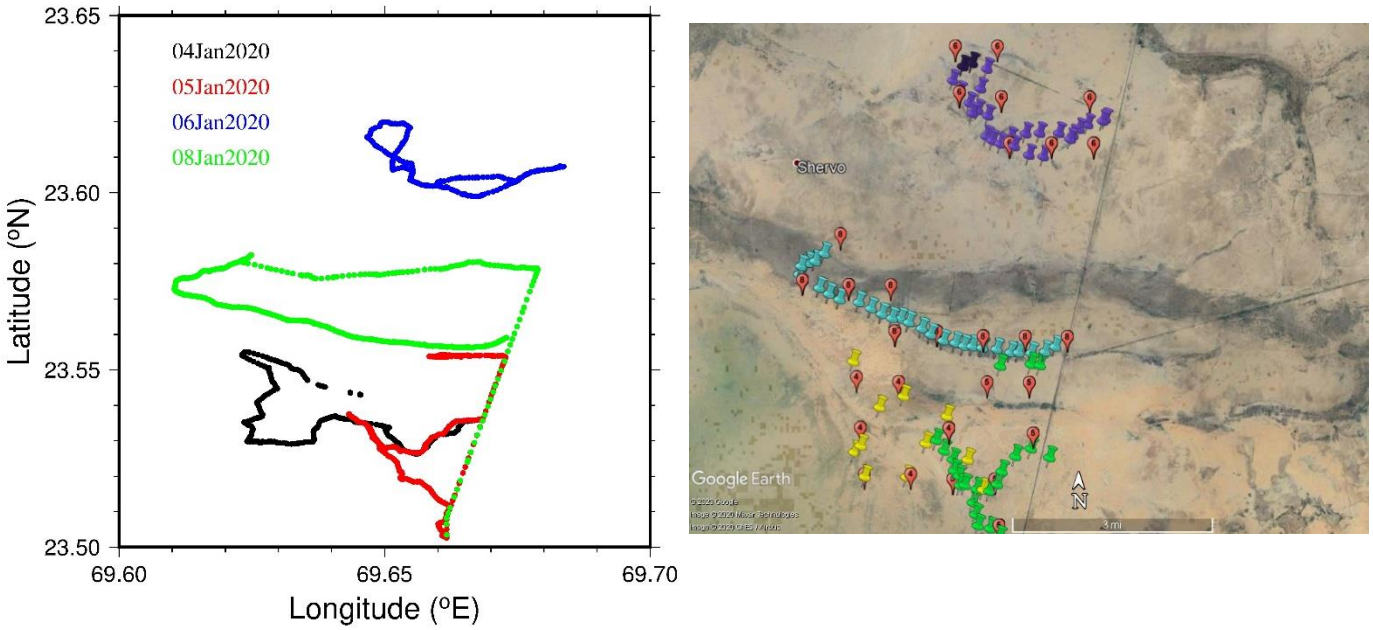

Figure 2(a). The campaign track for surface reflectance and atmospheric measurements.

Figure 2(b). Reflectance (18443) panel calibration with respect to master plate (18446).

The spectralon plate calibration was carried out during the day first on calibration campaign at 13:00 hrs. The setup is shown in Figure 2, total ten spectrum were recorded with 1-second interval. Without disturbing the set, the working plate was replaced with the master plate quickly. Ten spectrum were recorded with the master plate; the comparison of the averaged reflectance spectra is shown in Figure 3. The reflectance comparison of secondary, field plate (18443) with the master plate (18446) is shown in Figure 3. As the spectral reflectance are identical each other and close to one with error less than 0.5% with respect to the master plate, we considered the secondary reference plate is valid during the calibration campaign and calibration normalization was not performed. The two anomalies present in all the surface reflectance measurements are due to atmospheric watervapor absorption. The spectral response function of INSAT-3D (blue line) and INSAT-3DR (green line) for both the channels are also plotted, which indicates the channel selections are avoiding the atmospheric watervapor absorption effect. However, the error of spectral reflectance is considered for the total uncertainty estimation.

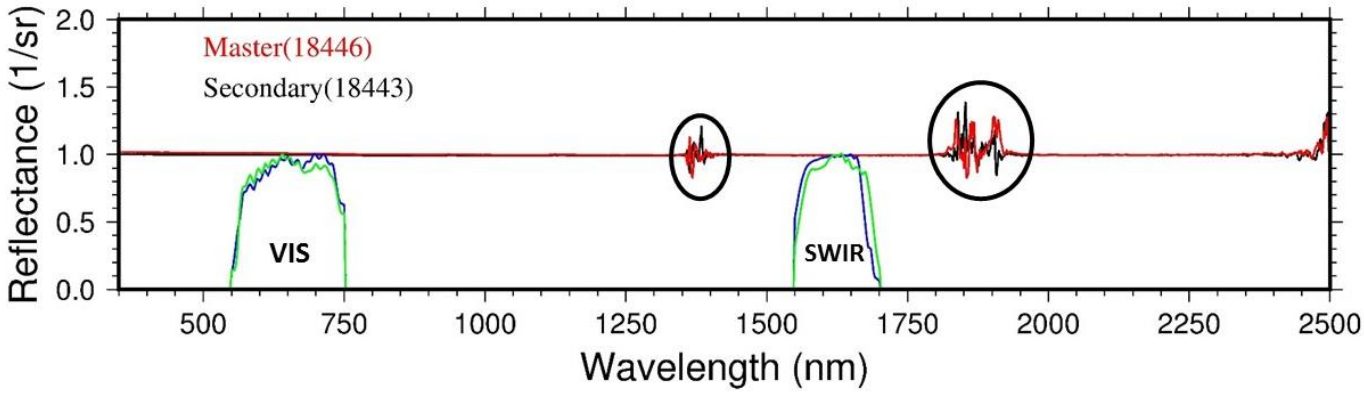

Figure 3. The field calibration plate comparison with the master plate (reference calibration).

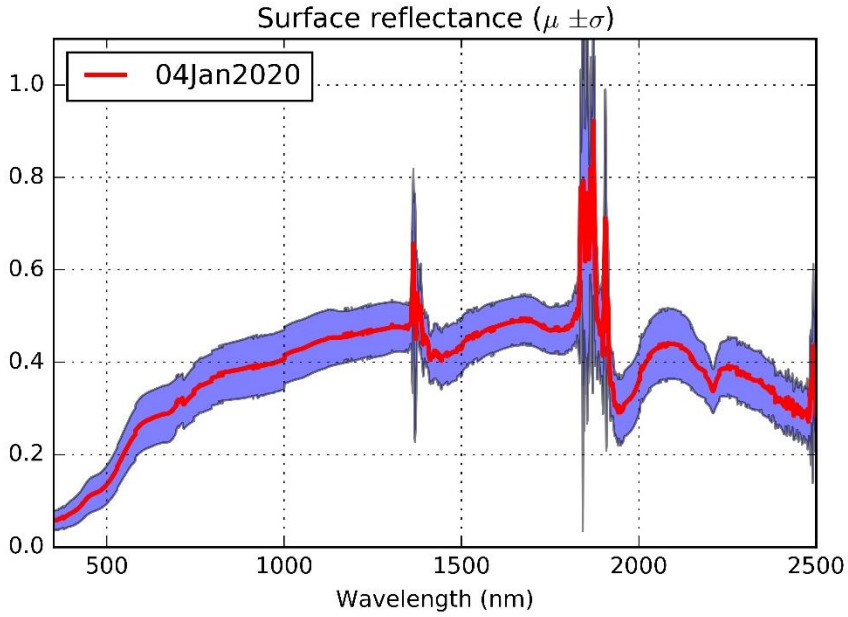

Figure 4(a). Mean and standard deviation of measured surface reflectance on 4th January 2020.

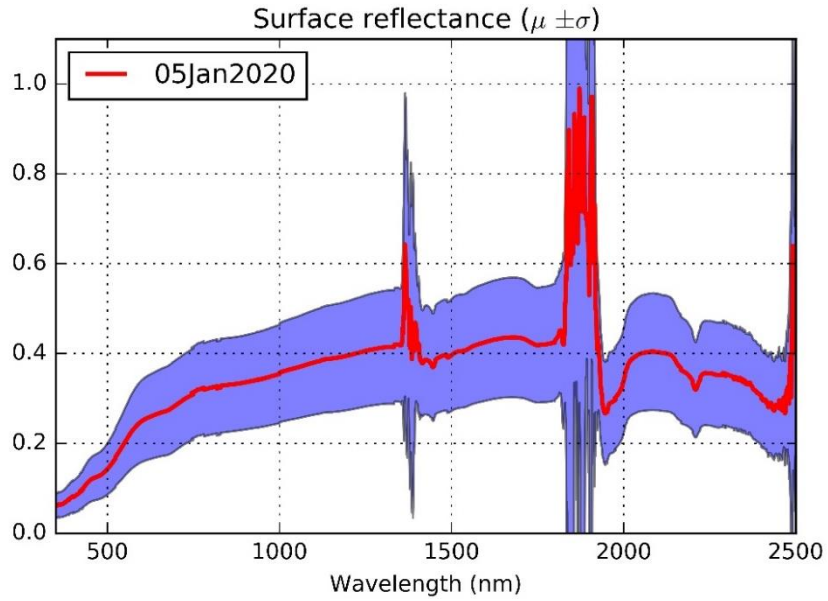

Figure 4(b). Mean and standard deviation of measured surface reflectance on 5th January 2020.

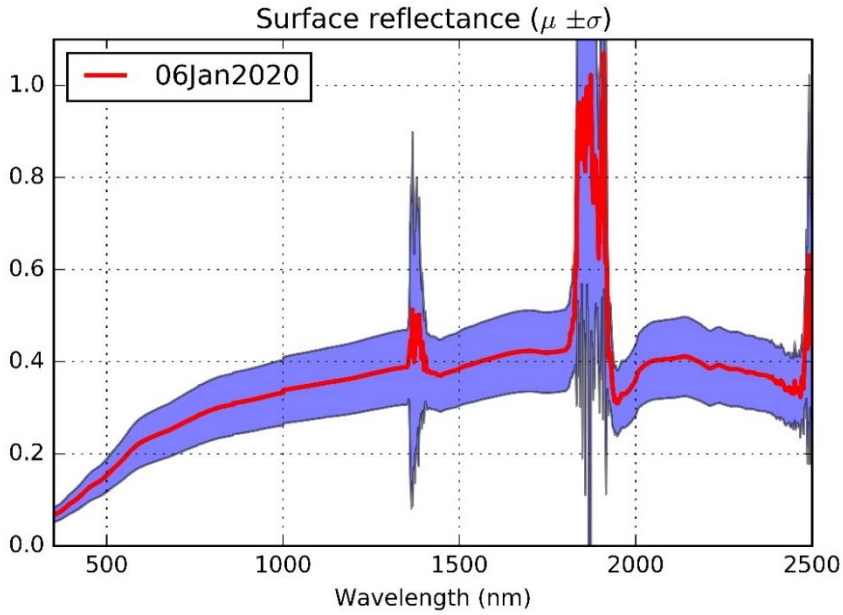

Figure 4(c). Mean and standard deviation of measured surface reflectance on 6th January 2020.

The measured surface reflectance spectra are averaged spectrally on daily basis to understand the spatial homogeneity in terms of surface reflectance as the area of measurements were changed on each day. The number of observations collected on 4th January was less (<15 nos.) as compared to other days, maximum number of surface reflectance were measured on 8th January. The characteristics nature of the surface is almost identical on all days, but minor change was observed on 6th January. The standard deviation values were higher for the measurements carried out on 5th and 6th January reflectance values. The variation in measured reflectances are due to surface heterogeneity, since the

measured reflectance are higher than 0.3 (minimum requirement of vicarious calibration) the site is considered for field campaign. However they are subjected for rejection criterion for the final calculation.

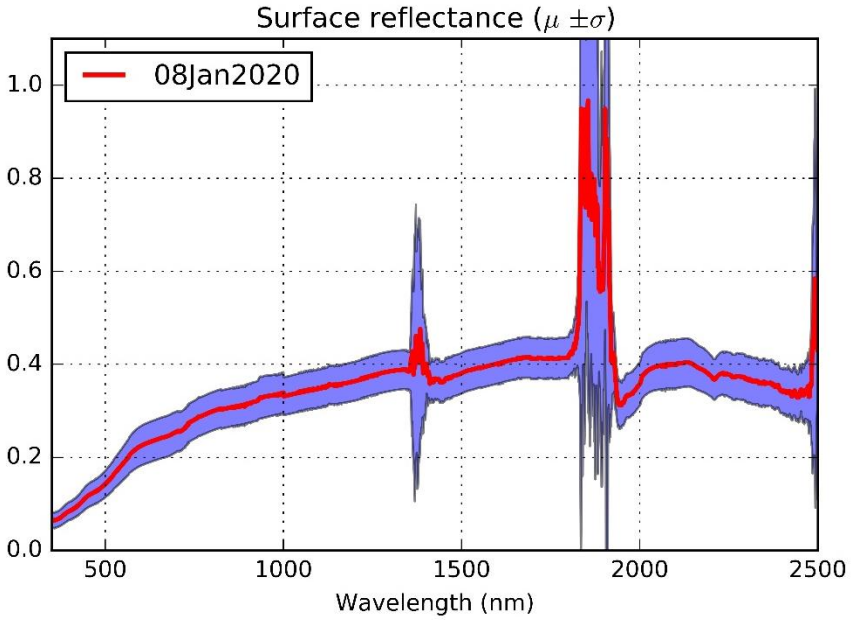

Figure 4(d). Mean and standard deviation of measured surface reflectance on 8th January 2020.

The Table 3 gives the atmospheric and surface condition observed during the field data collection campaign. Mostly the atmosphere was supported with very clear atmosphere with less aerosol loading and negligible dust event. The surface showed variability varying from uniform reflectance target to shrub condition, so the observations of surface reflectance were collected over varying surface characteristics. The reflectance spectra having abnormal trend were rejected in further analysis. The day four campaign (7th January 2020) was called off for measurement due to overcast of cloud induced by western disturbance.

Table 3. The day wise atmospheric and surface conditions encountered during the campaign.

Date	**Weather and surface condition**
04/01/2020	The atmosphere was reasonably stable and clear sky conditions prevailed during the campaign. The surface was mostly dry with patches of moist soil and some grassy areas. The ground reflectance spectrum was mostly collected over the dry surfaces to maintain uniformity.
05/01/2020	The atmosphere was reasonably stable and clear sky conditions prevailed during the campaign. The surface includes dry grassy areas, moist soil and patches of dry regions with mixed texture, many data collection points had dry grassy surface.
06/01/2020	The surface was dry and loose soil with some patches moist regions. The atmosphere was reasonably stable and clear sky conditions prevailed during the campaign.
07/01/2020	The western disturbance over north Pakistan & neighborhood caused cloudy sky conditions and the campaign was aborted on this day.

08/01/2020	The surface was dry and hard with some patches of loose soil with presence of moisture. The atmosphere was reasonably stable and clear sky conditions prevailed during the campaign.

The list of INSAT-3D and -3DR L1B data products used for further analysis and generation of calibration gain coefficient is shown in Table 4. As both the sensors collect radiance observations at every 30 minutes, the in-situ observations were commonly used for the analysis. However the measurements and satellite radiance products are optimally selected (±15 minutes with respect to in-situ observation) for modeling the final report generation.

Table 4. Date and time of ground data collection over the site and the covered INSAT-3D/-3DR imageries.

Date	No. of pass covered (3D/3DR)	INSAT-3D overpass (UTC/IST) at 30Min. interval	INSAT-3DR overpass (UTC/IST) at 30Min. interval
04th January 2020	5	06:00-08:00/11:30-13:30	06:15-08:15/11:45-13:45
05th January 2020	6	05:00-07:30/10:30-13:00	05:15-07:45/10:45-13:15
06th January 2020	6	05:00-07:30/10:30-13:00	05:15-07:45/10:45-13:15
08th January 2020	6	05:00-07:30/10:30-13:00	05:15-07:45/10:45-13:15

5. Data and methodology

INSAT-3D/-3DR standard full disk Level 1B data product (SAC/IMDPS/IPA/DPSG/MSDPD/TN-01/FEB) have been used to monitor the radiometric calibration stability (www.mosdac.gov.in). INSAT-3D/-3DR imager measures reflected solar radiation in terms of a digital number (DN) for each band and they are converted to TOA spectral radiance L(λ) values either using the lookup table (LUT) or using the calibration coefficients. The LUT provides mapping from DN to corresponding radiance values, which are provided as a filed name "Radiometric Calibration Type" in the data attribute. More details about the procedures for both the calibration coefficients are given in the INSAT-3D/-3DR data products (SAC/IMDPS/IPA/DPSG/MSDPD/TN-01/FEB). While estimating the radiance values the DNs should be inverted, if a field name "invert"=true in the attribute. The coefficients provided for DN to radiance conversion are used as follows:

$DN_{inv}=DN_{max}-DN$ ($onlyif$ invert=$true$) (1)

Where, DN_{inv} is the inverted DN value.

DN_{max} = 1023 for imager.

$(\lambda)(inmwcm-2sr-1\mu m-1) = labonline\_radiance\_quad/\cdot(DN)2+ labonline\_radiance\_scale\_factor/*DN$ (2)

Here, DN is digital numbers recorded by the sensor. The slope values (scale factor), offset and quadratic term to convert DN to radiance for each band are provided in the attribute.

Reflectance-based technique (Slater, et. al., 1987) is used in this report, because it is difficult to maintain the radiometric accuracy of the spectrometer that measures the surface radiance in the radiance-based technique. The reflectance-based technique mainly depends on the measured surface reflectance, which is the ratio of site measurement to those of a standard reflectance/ Spectralon panel for which the bidirectional reflectance factor is precisely determined. The vicarious radiometric calibration depends on the surface reflectance and radiance from the sun to earth's surface and earth's surface to sensor and atmospheric optical thickness over the calibration site at the time of satellite pass.

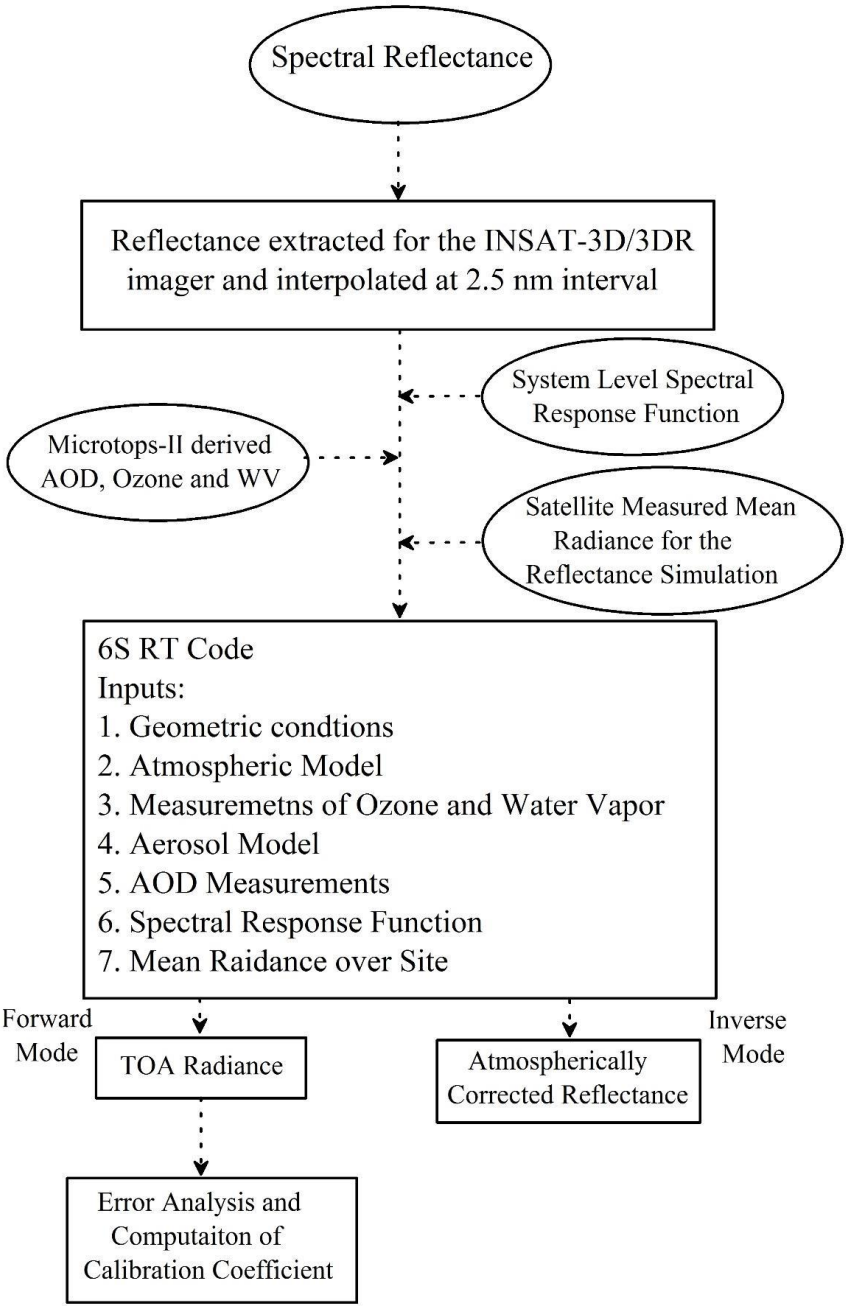

Figure 5. Flow chart of TOA spectral radiance simulation and estimation of calibration coefficient.

The ground measurements are used as an input for radiative transfer (RT) model for the simulation of absolute radiances in the required bands at the sensor level. The ground measurements are used to define the spectral directional reflectance of the surface and the spectral optical depth that are used to describe the aerosol and molecular scattering effect in the atmosphere (Gellman, et. al., 1991) along with this we used columnar water vapor.

We have used improved 6SV RT code (Kotchenova, et. al., 2008; Vermote, et. al., 2006) to compute the radiance field using ground measurements. 6SV RT code predicts the satellite signal at TOA level using ground reflectance measurements and atmospheric measurements of sunphotometer. In addition, 6SV RT model has spectral libraries for gaseous absorption and scattering by aerosols and molecules. 6SV deals better with atmospheric scattering than other RT models (Markham, et. al., 1992). **Figure-5** describes with flow diagram about the simulation of TOA spectral radiance and estimation of calibration coefficient. For the RT simulation to derive the vicarious calibration coefficient, the optimum selection of aerosol type is important. The actual aerosol characteristics are often differing from standard aerosol models in the RT codes. It is difficult to precisely estimate the aerosol characteristics in the field campaign. This leads to systematic errors in the calibration results (Chen, et. al., 2014). However, in the present study we have used handheld MicroTops-II sunphotometer for the measurements of AOD. This cannot provide other optical and physical properties of aerosols (e.g. volume size distribution, refractive indices etc.), which helps to improvise the aerosol parameterization in the RT model and leads to high accuracy of TOA spectral radiance simulation. However, due to lack of measurements, we have considered the continental aerosol model as a better representation of aerosol over calibration sites, which is the basic model over the land site.

Additionally, to reflect the characteristics of INSAT-3D/-3DR spectral bands, the normalized spectral response function (SRFs) are also used as inputs in the 6SV RT model to simulate the TOA spectral radiance. Both the SRF and measured surface reflectance data are resampled to 2.5 nm intervals using a spline interpolation method. The 6SV RT model computes TOA spectral radiance in the forward mode, while it computes atmospherically corrected surface reflectance in the inverse mode. 6SV RT model provides an output in the form of TOA spectral radiance, which is divided by the corresponding radiance observed by the INSAT-3D/-3DR for particular channel to yield calibration coefficients.

6. Atmospheric measurements

Since the algorithm employed radiative transfer calculations in the atmosphere, the specification of atmospheric conditions is necessary including the thermodynamic condition. However, we have measured aerosol optical depth (AOD), total columnar ozone (TCO) and total water vapour content (WVC) during field campaign. AOD measurements are carried out using a multi wavelength MicroTops-II sun-photometer (M/s. Solar Light Co., USA) at five different wavelengths at 380, 440, 500, 675 and 870 nm, from the solar instantaneous flux measurements with its internal calibration using the Langley method (Reagan, et. al., 1986; Scmid and Wehrli, 1995). The Full Width at Half Maximum (FWHM) bandwidth for the 380 nm channel is 2.4 ± 0.4 nm and 10 ± 1.5 nm for the other channels

(Morys, 2001). The AOT at 550 nm was then calculated via cubic interpolation from the AOT in the 440, 500, 675, 870, and 1020-nm channels.

MicroTops-II Ozonometer, a ground-based instrument, which is capable of measuring the columnozone (CO) using three UV channels (305.5, 312.5,320.0 nm) and the total water vapour content (WVC) using two near-IR channels (940 and 1020 nm) as well as AOD at 1020 nm is also used during the field campaigns. More details of design, performance, error and calibration of MicroTops-II is given elsewhere (Morys, 2001; Porter, et. al., 2001). Table-3shows the daily mean values of AOD at 500 nm, CO and WVC for all the measurement days over all three calibration sites.

Table 5. Daily mean values of aerosol optical depth at 550nm, Total column Ozone and Water Vapour content along with standard deviation.

Date	AOD @ 550 (nm)	Total columnar ozone (atm-cm)	Water vapour (g cm^{-2})
04/01/2020	0.460±0.043	0.235±0.029	0.791±0.066
05/01/2020	0.430±0.010	0.243±0.005	1.263±0.032
06/01/2020	0.326±0.010	0.238±0.003	1.200±0.041
08/01/2020	0.183±0.016	0.243±0.003	1.125±0.035

7. Results and Discussion

Attributing to their preferable stability of surface characteristics and atmospheric dynamics, pseudo invariant sites are commonly used for monitoring the radiometric performance stability, degradation monitoring and inter-comparisons (Chander et al. 2010; Bouvet 2014) especially for the satellite sensors without on-board calibration facilities. The Committee on Earth Observation Satellites (CEOS) working group on Calibration and Validation identified several test sites around the world (Teillet and Chander, 2010) based on the selection criteria, such as low probability of atmospheric variability, high spatial homogeneity, weak directional effects, flat reflectivity spectrum. Based on these criteria the above measurements were done over the desert sites in greater Rann of Kutch (GROK) which is ~10 x 10 km approximately. This section explains about the radiometric calibration stability of INSAT-3D and -3DR visible and SWIR channels. The temporal radiometric stability over one desert site and one ocean site for these channels were explained in report (SAC/EPSA/CVD/SR/11). The analysis of relative performance shows stability/degradation from inception to till September 2019. However this report shows the absolute performance using RT simulation results using the well qualified surface reflectance and atmospheric measurements.

Figure 6 shows the visible and SWIR channels TOA radiances of -3D and -3DR satellite and simulated radiance by RT model. Here the INSAT TOA radiance is box averaged value (3x3 pixels) rather than a single pixel. The 6S model simulation for each station locations are carried out, however the matchup points are subject to the following qualification criterion for rejection:

a. Unusually higher TOA radiance of INSAT pixel value

b. Higher standard deviation of 3x3 pixel values around the station
c. Higher deviation of measured surface reflectance in a day

Systematic trend of TOA variation with time of measurements were observed, the TOA bias among the measured and simulation is high for INSAT-3D visible channel. Moderate bias is observed for INSAT-3DR visible and SWIR channel and the bias is less for the INSAT-3D SWIR channel.

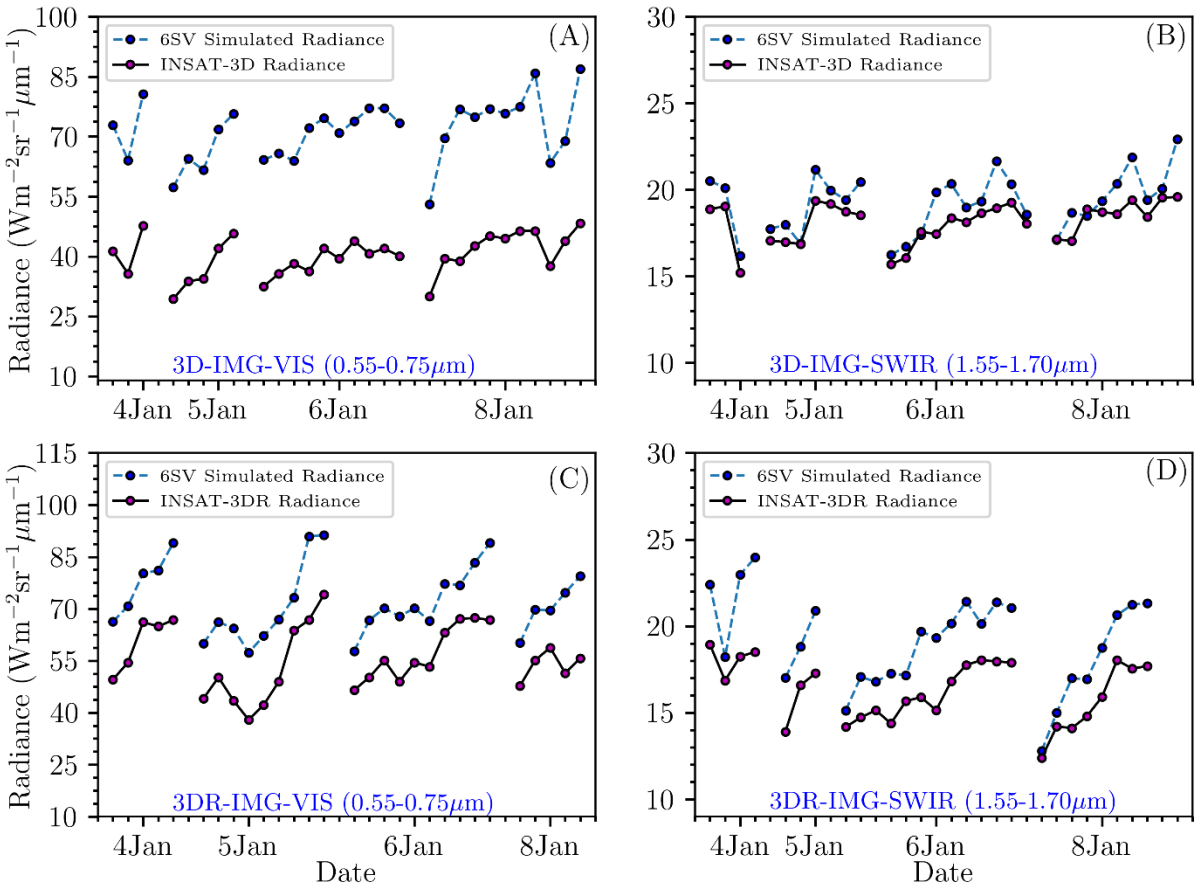

Figure 6. Panel (A, B) Temporal variation of INSAT-3D measured radiance and 6SV simulated radiance for IMG-VIS and IMG-SWIR bands; (C, D) Temporal variation of INSAT-3DR measured radiance and 6SV simulated radiance for IMG-VIS and IMG-SWIR bands.

Figure 7 shows the results of linear regression of TOA radiance in a combined form for IMG-VIS and IMG-SWIR bands of INSAT-3D & INSAT-3DR. The Figure 7 (A) and (B) indicates good correlation between INSAT-3D derived TOA radiance and 6SV simulated radiance, with R^2 values of 0.79 and 0.76 for IMG-VIS and IMG-SWIR respectively. The estimated RMSE value is found to be high 31.54 $Wm^{-2}sr^{-1}\mu m^{-1}$ for IMG-VIS band and 1.43 $Wm^{-2}sr^{-1}\mu m^{-1}$comparatively very small for IMG-SWIR band of INSAT-3D imager during this study. The absolute bias between the satellite measured radiance and 6SV simulated radiance are 30.96$Wm^{-2}sr^{-1}\mu m^{-1}$ and 1.17$Wm^{-2}sr^{-1}\mu m^{-1}$ for VIS and SWIR bands respectively.

The relative error (RE) between the 6SV simulated and INSAT-3D derived radiance are +43.85% and +5.61% for IMG-VIS and IMG-SWIR band. The correlation coefficient is found better in IMG-VIS compared to the IMG-SWIR. The Higher value of relative percentage error indicates that the 6SV simulated radiance and INSAT-3D measured radiance is not matching well. Detailed statistical results of the comparison of INSAT-3D and INSAT-3DR radiance are summarized in Table 5.

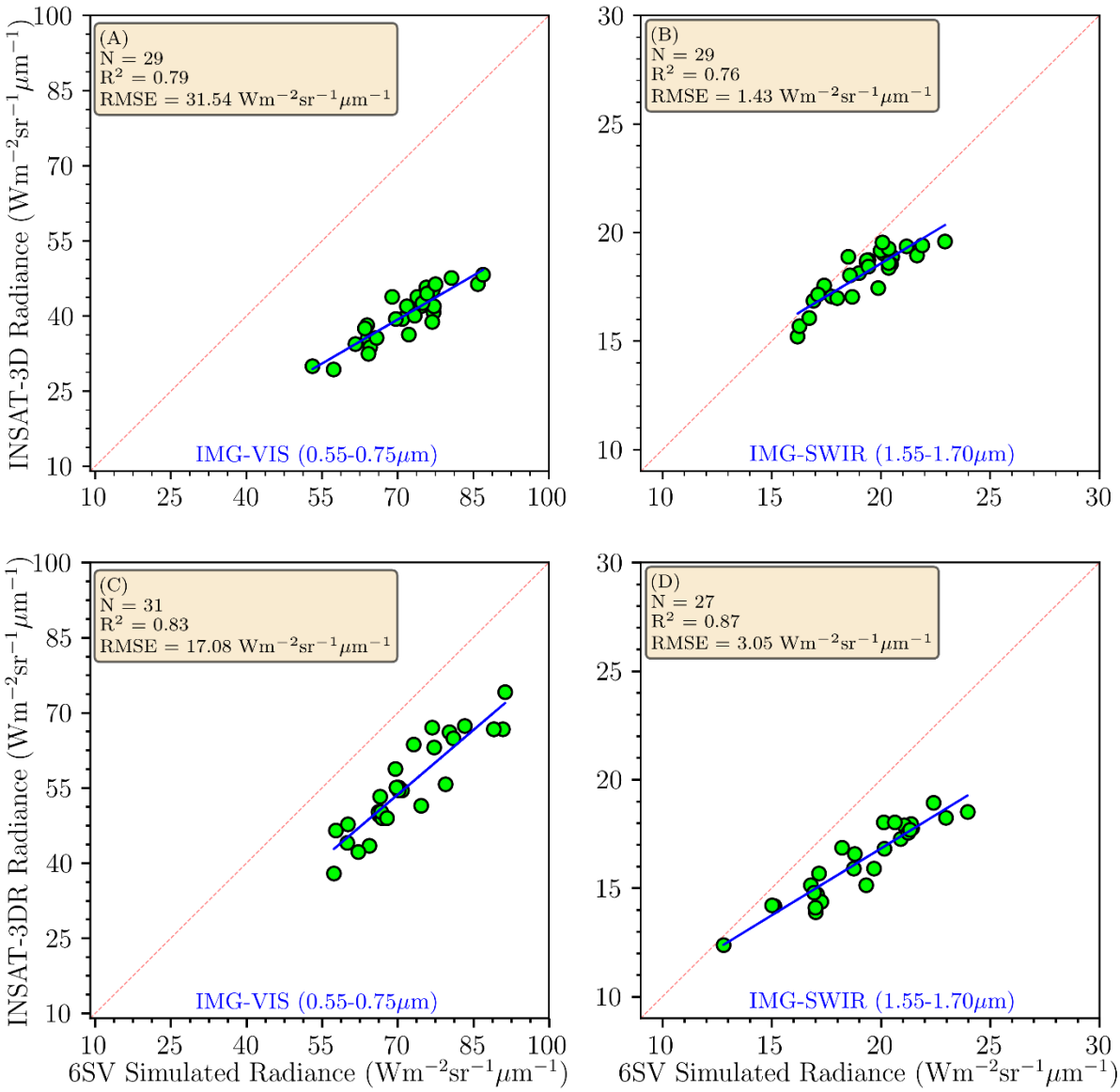

Figure 7. (A , B) Ccomparison between INSAT-3D measured TOA radiance and 6SV simulated TOA radiance for IMG-VIS and IMG-SWIR bands of INSAT-3D imager, (C, D) Ccomparison between INSAT-3DR measured TOA radiance and 6SV simulated TOA radiance for IMG-VIS and IMG-SWIR bands of INSAT-3DR imager.

Table 6. Summary of statistical results of comparison between INSAT-3D & INSAT-3DR measured radiance and 6SV simulated radiance for IMG-VIS and IMG-SWIR bands over GROK site**.**

Satellite	Bands	R^2	Absolute bias	RMSE	RE (%)	Standard deviation
			($Wm^{-2}sr^{-1}\mu m^{-1}$)			
INSAT-3D	IMG-VIS	0.79	30.96	31.54	43.85	3.27
	IMG-SWIR	0.76	1.17	1.43	5.61	4.05
INSAT-3DR	IMG-VIS	0.83	16.79	17.15	23.22	5.48
	IMG-SWIR	0.87	2.97	3.05	14.27	4.94

Figure 7 (C) & (D) describe the correlation between INSAT-3DR measured radiance and 6SV simulated radiance for IMG-VIS and IMG-SWIR respectively. The result shows a good statistical agreement between INSAT-3DR measured radiance and 6SV simulated radiance with values of R^2 0.83 and 0.87 for VIS and SWIR bands respectively. The bias between satellite derived radiance and 6SV simulated radiance are $16.79 Wm^{-2}sr^{-1}\mu m^{-1}$ and $2.97 Wm^{-2}sr^{-1}\mu m^{-1}$ for VIS and SWIR bands respectively. The relative percentage error between Satellite derived radiance and simulated radiance 17.15% and 3.05% are observed.

Figure 8 (A) & (B) describes the daily mean and variance of INSAT-3D measured radiance and 6SV simulated radiance for IMG-VIS and IMG-SWIR respectively. From Figure 8 (A), it has been observed that INSAT-3D imager radiance data is highly underestimating the 6SV simulated radiance data for VIS channel. The daily variation of radiance values from INSAT-3D imager and 6SV model over calibration site (great Rann Of Kutch) are in range from 37-42 $Wm^{-2}sr^{-1}\mu m^{-1}$ and 66-73 $Wm^{-2}sr^{-1}\mu m^{-1}$ respectively, which depicts high variation of radiance through the study period over the experimental site. As well as the difference between INSAT-3D imager derived radiance and 6SV simulated radiance is found to be high ($30.96 Wm^{-2}sr^{-1}\mu m^{-1}$). Similarly, from Figure 8(B) it is found that INSAT-3D imager radiance data is slightly underestimating the 6SV simulated radiance data for SWIR channel. The daily variation of radiance values from INSAT-3D imager and 6SV model over the site are in range from 17.7-18.9 $Wm^{-2}sr^{-1}\mu m^{-1}$ and 18.7-20.3 $Wm^{-2}sr^{-1}\mu m^{-1}$ respectively. It is found that INSAT-3D imager derived radiance values are slightly underestimating the 6SV simulated radiance values for all four observation days.

Figure 8 (C, D) illustrates the daily mean and variance of INSAT-3DR measured TOA radiance and 6SV simulated TOA radiance for IMG-VIS and IMG-SWIR. It is found that the difference between the radiance measured by INSAT-3DR imager and 6SV model for IMG-VIS is higher than IMG-SWIR, which is shown in figure 8(C). The daily variation of radiance values from INSAT-3DR imager and 6SV model for IMG-VIS over the site are in the range from 52-60 $Wm^{-2}sr^{-1}\mu m^{-1}$ and 70-77 $Wm^{-2}sr^{-1}\mu m^{-1}$ respectively. Whereas Figure 8 (D) shows the comparison between the INSAT-3DR derived mean radiance and 6SV simulated mean radiance for SWIR channel in the range of 15-18 $Wm^{-2}sr^{-1}\mu m^{-1}$ and 17-22 $Wm^{-2}sr^{-1}\mu m^{-1}$respectively. Here also INSAT-3DR derived radiance values are

underestimating the 6SV simulated radiance values for all four observation days during this study period.

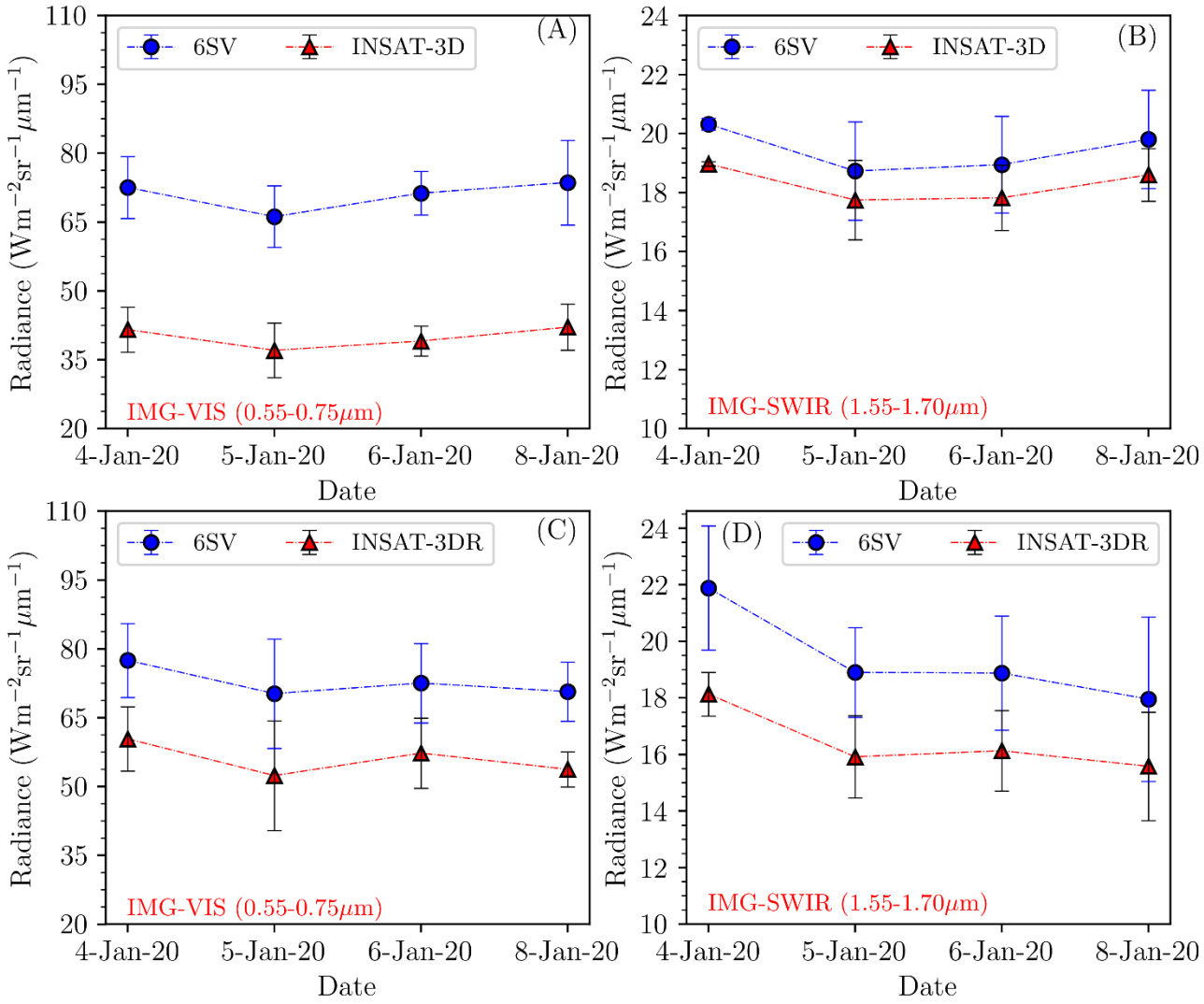

Figure 8. (A, B) Daily mean variation of INSAT-3D measured and 6SV simulated TOA radiance for IMG-VIS and IMG-SWIR bands of INSAT-3D imager, (C,D) Daily mean variation of INSAT-3DR measured and 6SV simulated TOA radiance for IMG-VIS and IMG-SWIR bands of INSAT-3DR imager.

If the ratio value has any deviation from the unity, it indicates the change in sensor calibration coefficient. In this study, we took a ratio of mean radiance values for a particular day from both the platform. Figure 9 describe the temporal variation of vicarious gain coefficient for IMG-VIS and IMG-SWIR channel of INSAT-3D and INSAT-3DR imager over the calibration site for all four days. Figure 9(A) and (B) describe the daily variation of estimated vicarious calibration gain coefficients for IMG-VIS and IMG-SWIR bands of INSAT-3D for all four days during this study period. From Figure 9 it

can be seen the gain coefficient for VIS channel is relatively higher due to the inhomogeneity of the ground target caused by sufficient sub-surface soil moisture. Whereas, the gain coefficient for SWIR channel has relatively a lesser amount of value in comparison to VIS channel. Table 7 describes the daily mean simulated TOA radiance, INSAT-3D measured TOA radiances and Calibration coefficient derived from measurement at the GROK site for the VIS and SWIR channels.

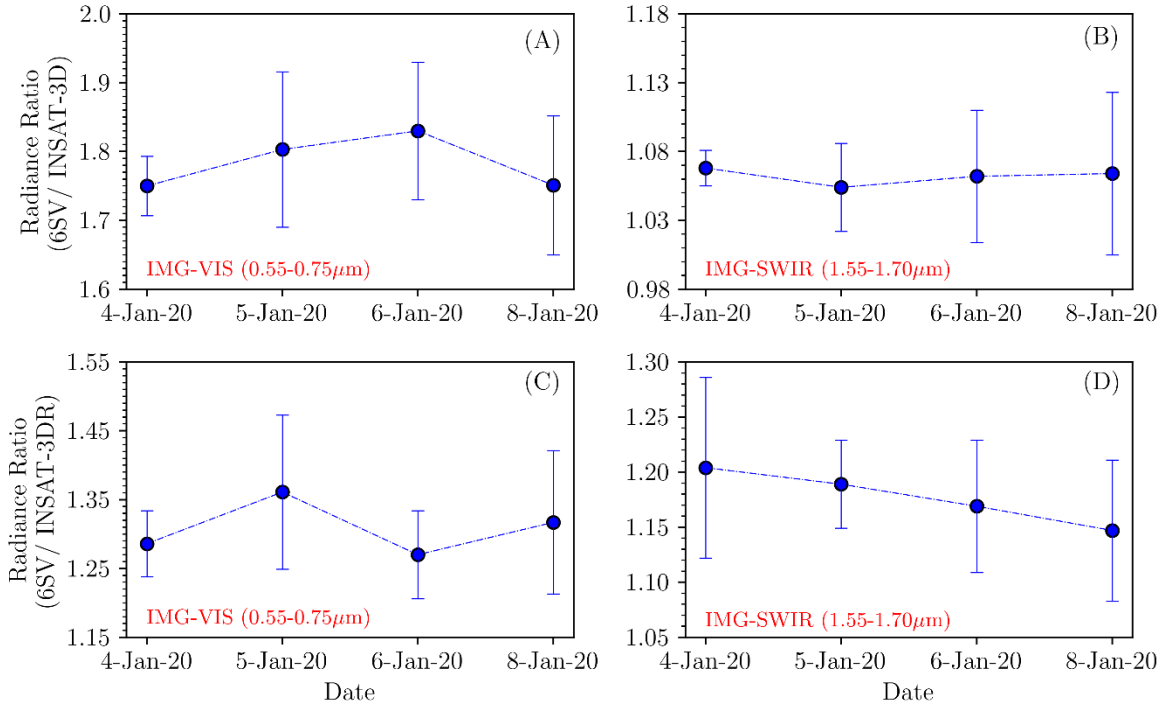

Figure 9. (A, B) Daily variation of estimated vicarious calibration coefficients for IMG-VIS and IMG-SWIR bands of INSAT-3D for all four days; (C,D) Daily variation of estimated vicarious calibration coefficients for IMG-VIS and IMG-SWIR bands of INSAT-3DR for all four days.

It can be seen from Figure 9(C) & (D) that the calibration coefficient for VIS and SWIR bands of INSAT-3DR imager are found in the range of 1.27-1.34 and 1.15-1.21 during the study period respectively. Table 8 lists the INSAT-3DR measured at-sensor and TOA predicted spectral radiance values for VIS and SWIR bands, the relative percent error between the two values and the calibration coefficients for all four days. Table 8 gives a clear understanding of the performance of VIS and SWIR channels of INSAT-3DR imager. The data show significant difference between the two measurements and demonstrate that the 3D and 3DR imager response is degraded with respect to the predicted response in both bands.

Table 7. Shows the radiometric performance of INSAT-3D over the in-situ measurement target against 6SV simulated radiances during the four clear-sky days.

Date	Bands	INSAT-3D Radiance ($W\ m^{-2}\ sr^{-1}\ \mu m^{-1}$)	6SV simulated radiance ($W\ m^{-2}\ sr^{-1}\ \mu m^{-1}$)	Relative errors in radiance (%)	Vicarious gain coefficient
4th January 2020	VIS	41.55	72.53	42.71	1.75
	SWIR	18.97	20.31	6.63	1.07
5th January 2020	VIS	37.05	66.17	44.01	1.79
	SWIR	17.75	18.73	5.25	1.06
6th January 2020	VIS	39.07	71.3	45.2	1.82
	SWIR	17.82	18.95	5.94	1.06
8th January 2020	VIS	42.09	73.61	42.82	1.75
	SWIR	18.6	19.81	6.1	1.07

Table 8. Shows the radiometric performance of INSAT-3DR over the in-situ measurement target against 6SV simulated radiances during the four clear-sky days.

Date	Bands	INSAT-3DR Radiance ($W\ m^{-2}\ sr^{-1}\ \mu m^{-1}$)	6SV simulated radiance ($W\ m^{-2}\ sr^{-1}\ \mu m^{-1}$)	Relative errors in radiance (%)	Vicarious gain coefficient
4th January 2020	VIS	60.38	77.5	22.09	1.28
	SWIR	18.13	21.89	17.14	1.21
5th January 2020	VIS	52.39	70.25	25.43	1.34
	SWIR	15.92	18.9	15.78	1.19
6th January 2020	VIS	57.29	72.54	21.03	1.27
	SWIR	16.13	18.88	14.55	1.17
8th January 2020	VIS	53.76	70.7	23.95	1.31
	SWIR	15.58	17.96	13.23	1.15

8. Conclusion

The radiometric performance of INSAT-3D & -3DR visible and SWIR channels have been evaluated based on datasets acquired at the GROK site from 4th January2020 to 8th January 2020 during a special calibration campaign. In this report, a ground reflectance-based approach has been used to carry out the vicarious radiometric calibration of INSAT-3D/3DR imager. The vicarious absolute radiometric

calibration results of the ground reflectance-based approach show slightly larger difference when comparing the predicted and observed VIS band TOA radiance values for INSAT-3D/3DR imager. The relative errors of the VIS bands of INSAT-3D and INSAT-3DR imager are within 44% and 23% respectively when compared with the simulated RT TOA radiance values. However, the results also show that the relative errors of the SWIR bands of INSAT-3D and INSAT-3DR imager are within 5.6% and 14.3% respectively. Overall, the results of the vicarious radiometric calibration obtained using the ground reflectance-based approach have been demonstrated that the IMAGER onboard the INSAT-3D/3DR satellite displays substantial degradation in radiometric performance, particularly at VIS channel as compared to previous calibration exercises (SAC/EPSA/CVD/CAL-VAL/2017/003; Piyushkumar N. Patel, 2016).

The correlation coefficient between INSAT-3D derived TOA radiance and 6SV simulated radiance is 0.79 (visible) and 0.76 (SWIR). The estimated RMSE value is found to be high 31.54 $Wm^{-2}sr^{-1}\mu m^{-1}$ for IMG-VIS band and 1.43 $Wm^{-2}sr^{-1}\mu m^{-1}$ IMG-SWIR band. The absolute bias and relative error between the satellite measured radiance and 6SV simulated radiance are 30.96$Wm^{-2}sr^{-1}\mu m^{-1}$ (43.85%) and 1.17$Wm^{-2}sr^{-1}\mu m^{-1}$ (5.61%) for VIS and SWIR bands respectively. The correlation between INSAT-3DR measured radiance and 6SV simulated radiance for IMG-VIS/IMG-SWIR are 0.83/0.87. The absolute bias value is 16.79$Wm^{-2}sr^{-1}\mu m^{-1}$ and 2.97$Wm^{-2}sr^{-1}\mu m^{-1}$ for INSAT-3DR VIS and SWIR with relative percentage errors 17.15% and 3.05%.

Acknowledgement

The authors gratefully acknowledge the encouragement received from Director, SAC and Associate Director SAC for carrying out the present research work. Valuable suggestions received from Deputy Director, EPSA are also gratefully acknowledged. Author are also thankful to IMD scientific staffs who participated and helped for data collection at calibration site. The authors would also like to acknowledge and thank Cal-Val team.

References:

Babu, K. N., and Nandkishor, 2019. INSAT-3D and INSAT-3DR VIS and SWIR channel performance monitoring through top-of-the-atmosphere radiance over Desert and Ocean target. SAC/EPSA/CVD/SR/11, November 2019, 32pp.

Belward, S., 1999. International co-operation in satellite sensor calibration; the role of the GEOS working group on calibration and validation, Adv. Space Res., vol. 23, no. 8, pp. 1443–1448.

Bouvet, M., 2014. Radiometric comparison of multispectral imagers over a pseudo-invariant calibration site using a reference radiometric model. Remote Sens. Environ. 140, 141–154.

Butler, J. J., and Barnes, R. A., 1998. Calibration strategy for the Earth Observing System (EOS)- AM1 platform," IEEE Trans. Geosci. Remote Sens., vol. 36, no. 4, pp. 1056–1061.

Chander, G., Xiong, X., Choi, T., Angal, A., 2010. Monitoring on-orbit calibration stability of the Terra MODIS and Landsat 7 ETMþ sensors using pseudo-invariant test sites. Remote Sens.

Chen, Z., Zhang, B., Zhang, H., Zhang, W., 2014. Vicarious calibration of Beijing-1 multispectral imagers. Remote Sens. 6, 1432–1450, http: //dx.doi.org/10.3390/rs6021432.

Dinguirard, M., and Slater, P. A., 1999. Calibration of space-multispectral imaging sensors: A review,Remote Sens. Environ., vol. 68, no. 3, pp. 194–205, Jun. 1999.

Gellman, D.I., Biggar, S.F., Slater, P.N., Bruegge, C.J., 1991. Calibrated intercepts for solar radiometers used in remote sensor calibration. Proc. SPIE 1493, 19–24.

Hagolle, O., et. al., 1999. Results of POLDER in-flight calibration, IEEE Trans. Geosci. Remote Sens., vol. 37, no. 3, pp. 1550–1566, May 1999.

INSAT-3D Data Products Format Document, 2014. Version 1.1. SAC/IMDPS/SIPA/DPSG/MSDPD/ TN-01/FEB 2014. ⟨www.mosdac.gov.in/Missions/ docs/INSAT3D_Products.pdf⟩.

Kotchenova, S.Y., Vermote, E.F., Levy, R., Lyapustin, A., 2008. Radiative transfer codes for atmospheric correction and aerosol retrieval: intercomparison study. Appl. Opt. 47 (13), 2215–2226.

Liang, S., 2004. Quantitative Remote Sensing of Land Surface. New York, NY, USA: Wiley, pp. 178–194.

Markham, B.L., Halthore, R.N., Goetz, S.J., 1992. Surface reflectance retrieval from satellite and aircraft sensors: results of sensor and algorithm comparison during FIFE. J. Geophys. Res. 97. (D17718), 7857795.

Morys, M., Mims III, F.M., Hagerup, S., Anderson, S.E., Baker, A., Kia, J., Walkup, T., 2001. Design, calibration, and performance of MICROTOPS II handheld ozone monitor and Sun photometer. J. Geophys. Res. 106 (D13), 14573–14582.

Piyushkumar N. Patel, Hiren Bhatt, Mathur, A. K., Prajapati, R. P., Geetika Tyagi, 2016. Reflectance-based vicarious calibration of INSAT-3D using high-reflectance ground target, J. Remote Sensing Applications: Society and Environment, 3, 20-35.

Piyushkumar N. Patel, Babu, K. N., Prajapati, R. P., Praful Saudagare, Mathur, A. K., 2017. The vicarious calibration of VIS and SWIR channels of INSAT-3D and INSAT-3DR over desert sites. SAC/EPSA/CVD/CAL-VAL/2017/003.

Reagan, J.A., Thomason, L.W., Herman, B.M., Palmer, J.M., 1986. Assessment of atmospheric limitations on the determination of the solar spectral constant from ground-based spectroradiometer measurements. IEEE Trans. Geosci. Remote Sens. GE-24, 258– 266.

Schmid, B., Wehrli, C., 1995. Comparison of sun photometer calibration by use of the Langley technique and standard lamp. Appl. Opt. 34, 4500–4512.

Slater, P.N., Biggar, S.F., Holm, R.A., Jackson, R.D., Mao, Y., Moran, M.S., Palmer, J.M., Yuan, B., 1987. Reflectance- and radiance-based methods for in-flight absolute calibration of multispectral sensors. Remote Sens. Environ. 22, 11–37.

Teillet, P., Chander, G., 2010. Terrestrial reference standard sites for post-launch sensor calibration. Can. J. Remote Sens. 36, 437–450

Vermote, E.D., Tanre, J.L., Deuze, M., Herman, J.J., Morcrette, Kotchenova, S.Y., 2006. Second Simulation of Satellite Signal in the Satellite Spectrum (6S). 6S User Guide Version 3. University of Maryland.